Optical Materials 35 (2013) 1230–1235

Contents lists available at SciVerse ScienceDirect

Optical Materials

journal homepage: www.elsevier.com/locate/optmat

Influence of annealing temperature on the electron–lattice coupling strength in terbium doped yttrium alumina perovskite xerogels embedded in nano-porous anodic alumina

G. Zatryb [a], A. Podhorodecki [a,*], M. Banski [a], J. Misiewicz [a], N.V. Gaponenko [b]

[a] Institute of Physics, Wroclaw University of Technology, Wybrzeze Wyspianskiego 27, 50-370 Wroclaw, Poland
[b] Belarusian State University of Informatics and Radioelectronics, P. Browka St. 6, 220013 Minsk, Belarus

ARTICLE INFO

Article history:
Received 21 October 2012
Received in revised form 13 January 2013
Accepted 19 January 2013
Available online 26 February 2013

Keywords:
Electron
Phonon
Coupling
Terbium
Xerogel
Porous

ABSTRACT

Terbium doped $YAlO_3$ xerogels were synthesized and spin-coated onto porous anodic alumina substrates. After deposition the films were annealed at temperatures between 400 and 1000 °C. The influence of the annealing temperature on terbium emission and the terbium excitation mechanism were investigated by means of photoluminescence, photoluminescence decay and photoluminescence excitation spectroscopy. It was found that both photoluminescence lifetime and the energy difference between spin-forbidden and spin-allowed 4f–5d transitions decreases with the annealing temperature drop. This dependence was correlated to the electron–lattice coupling strength calculated as a function of annealing temperature.

1. Introduction

The development of a sol–gel technology used for the fabrication of advanced light-emitting materials has received considerable attention due to the cost-efficiency of the method as well as the ability to adjust the structural and physical properties of the material. The sol–gel technology allows for the fabrication of solid films from liquid colloidal solutions, particularly xerogels doped with various lanthanide (Ln^{3+}) ions. Significantly, sols with a low viscosity can penetrate the mesoscopic channels of porous silicon, artificial opals, porous anodic alumina and other porous materials, resulting in a xerogel formation inside the pore volume [1].

Among various porous materials, porous anodic alumina (PAA) has received growing interest due to low fabrication cost, optical transparency in the visible and infrared ranges as well as mechanical and thermal durability. PAA is known to exhibit regular pore morphology, with the pores placed at the center of approximately hexagonal cells whose size can be adjusted [2]. Moreover, due to the structural regularity of the pores, PAA can be considered as a two-dimensional photonic crystal [3,4]. In PAA, photon density of states (DOS) is redistributed over a solid angle to give maximum DOS along pore axes (direction of high transmission) and minimal DOS within the plane normal to pore axes (direction of high reflection) [5]. This effect could be used to enhance light propagation along the axes parallel to the pores. In this way, if the channels of PAA were filled with a lanthanide doped xerogel emitting light at a certain wavelength, highly directional, multicolor luminescent images could be obtained [6]. Recently, applications of PAA for LCD panel displays have been proposed [7]. However, in order to put these ideas into practice, one must examine the optical properties of a sol–gel material placed inside of the PAA pores. In this work we examine PAA structures filled with Tb-doped $YAlO_3$ xerogel (green light emitter). The main aim of this study is to explain excitation and emission mechanism of Tb ions in these structures and to find factors limiting the radiative recombination of Tb.

Among various factors affecting the optical properties of Ln^{3+}-doped materials, the host-matrix crystal structure and the Ln^{3+} local environment are the most important. Depending on the Ln^{3+} ion environment, the oscillator strength of $4f \leftrightarrow 4f$ and $4f \leftrightarrow 5d$ transitions could be influenced [8], leading to significant changes of the structure emission and absorption properties. Moreover, the structural environment of the ion may affect the electron–lattice coupling strength [9]. This is also an important issue, since in the case of a strong electron–lattice coupling an efficient multiphonon relaxation of the excited ion occurs [10], limiting light output from a hypothetical device. In our experiment, the structural properties (e.g. the xerogel crystallinity) can be controlled by depositing a set of samples annealed at various temperatures

* Corresponding author. Tel.: +48 71 320 23 58.
E-mail address: artur.p.podhorodecki@pwr.wroc.pl (A. Podhorodecki).

0925-3467/$ - see front matter © 2013 Elsevier B.V. All rights reserved.
http://dx.doi.org/10.1016/j.optmat.2013.01.031

[11]. In this study, we synthesized terbium (Tb^{3+}) doped $YAlO_3$ (YAP) xerogels, which were spin-coated onto PAA substrates and annealed at 400–1000 °C temperature range. The pores morphology was kept constant for all the samples. The optical properties of these structures were then experimentally examined by means of photoluminescence, time-resolved photoluminescence and temperature-dependent photoluminescence excitation spectroscopy. We showed that both emission and absorption properties are strongly influenced by the annealing. This effect was ascribed to changes of the local Ln^{3+} environment, which was also found to affect the electron–phonon coupling strength for the dominant spin allowed $4f^8 \rightarrow 5d_14f^7$ transition of Tb. We have shown that this transition strongly couples to lattice vibrational modes and the coupling strength increases with the annealing temperature drop.

2. Experimental

A super-pure aluminum was magnetron-sputtered onto a planar side of a polished wafer of monocrystalline silicon. Aluminum was completely anodized in a 1.2 M orthophosphoric acid solution at a constant temperature of 17 °C and a constant voltage of 130 V. As obtained from scanning electron microscopy, the PAA thickness was equal to 9 μm, and the average pore diameter was equal to 140 nm. Terbium doped yttrium-alumina oxides were prepared by stage-by-stage dissolution of nitrate salts (Sigma–Aldrich) $Y(NO_3)_3{\cdot}4H2O$ (99.99% purity), $Al(NO_3)_3{\cdot}9H_2O$ (98% purity) and $Tb(NO_3)_3{\cdot}5H_2O$ (99.9% purity) in an aqueous-alcoholic solution, with pH adjusted to 2 with diluted nitric acid. As a stabilizer, citric acid in the molar ratio [metal ions]/[citric acid] = 1/3 was used. Terbium-containing solution was deposited on PAA templates by sequential spinning at a rate of 2700 rpm, followed by drying at 200 °C, and a final 30 min. annealing at temperatures of 400, 900 and 1000 °C (under air). The determined Tb concentration in the samples is 3.95 at.%. Moreover, as it was shown by X-ray diffraction [12], matrix annealed at T_a = 400 °C is completely amorphous. For T_a = 900 °C and T_a = 1000 °C matrix crystallizes and $YAlO_3$ phase is formed with a small admixture of Al_2O_3 phase as well. It should also be emphasized that the structural parameters of PAA templates (e.g. pore size, pore density and pore depth) were kept constant for all of the spin-coated samples. This allowed for a qualitative comparison of the optical properties between the samples annealed at different temperatures, without considering the influence which the pores may have on light generation or light propagation in the structures. Moreover, as determined by a cross-sectional SEM experiment, the fill-factor of the pores is about 25% and the filling is non-uniform (the pores are not completely filled out).

For photoluminescence (PL) and photoluminescence excitation (PLE) a xenon lamp (450 W) connected to a monochromator (Jobin Yvon TRIAX 180) was used as the excitation source. PL and PLE signals were collected by an optical fiber coupled to the CCD camera (HR4000 Ocean Optics). In the case of the PLE, the obtained signals were divided by the light source spectral intensity profile. The PLE measurements were performed as a function of temperature in the 10–300 K range (spectra were collected every 10 K), using closed-cycle (helium) cooler. The flash xenon lamp and PMT detector coupled with monochromators (Photon Technology International) were used for PL decay measurements.

3. Results and discussion

The low temperature (T = 10 K) PL spectra of YAP:Tb^{3+}/PAA structures obtained for λ_{EXC} = 270 nm excitation wavelength (4.59 eV) are shown in Fig. 1 as a function of the annealing temperature T_a (for T_a equal to 400, 900 and 1000 °C). For each sample,

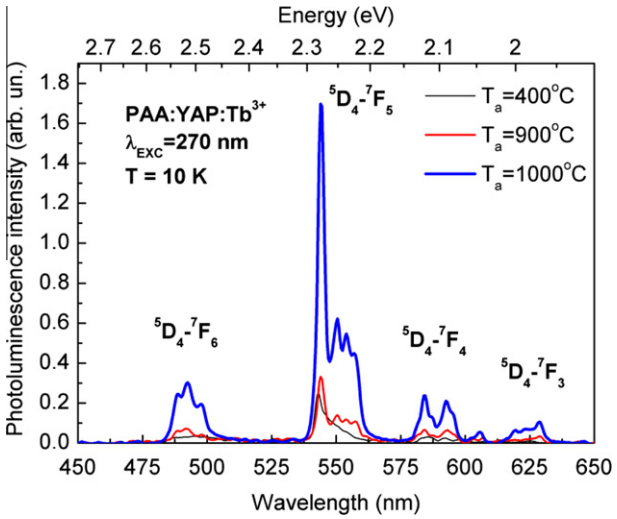

Fig. 1. Photoluminescence spectra measured at low temperature (T = 10 K) for samples annealed at 400, 900 and 1000 °C.

four main PL bands can be seen that originate from radiative transitions between Stark-split intra-4f energy levels of Tb^{3+} ions. The observed transitions are $^5D_4$–$^7F_6$ (492 nm), $^5D_4$–$^7F_5$ (544 nm), $^5D_4$–$^7F_4$ (587 nm) and $^5D_4$–$^7F_3$ (625 nm) [13], with $^5D_4$–$^7F_5$ transition being the most intensive. Fig. 1 also shows that rise of the annealing temperature results in significant enhancement of the PL intensity. As it was shown in our previous paper [12], for T_a = 400 °C the matrix is completely amorphous whereas for T_a = 900 °C and T_a = 1000 °C crystallization occurs and $YAlO_3$ polycrystalline phase is formed inside the anodic alumina pores, with small admixture of Al_2O_3 phase. Thus, the crystalline quality of the matrix is closely correlated to the emission intensity of the structures.

Fig. 2 shows photoluminescence excitation (PLE) spectra obtained as a function of temperature (only 10 K, 150 K and 300 K are shown for clarity reasons) for samples annealed at 1000, 900 and 400 °C. The PLE spectra were obtained by integrating the narrow emission line at 544 nm (2.28 eV) for each excitation wavelength. In general, three main excitation bands can be seen, centered at around 3.8, 4.6 and 5.3 eV. The bands position changes slightly from sample to sample. The 3.8 eV and 4.6 eV bands may be attributed to forbidden high-spin ($5d_1$HS) and allowed low-spin ($5d_1$LS) $4f^8 \rightarrow 5d_14f^7$ transitions [14], respectively ($5d_i$ denotes the i-th 5d energy level, in order of increasing energy). Furthermore, the 5.3 eV band may be attributed to the allowed low-spin ($5d_2$LS) $4f \rightarrow 5d_2$ transition. Similar excitation bands have been observed earlier [15]. It can be thus concluded that in the investigated structures the most effective excitation mechanism is through f–d transitions.

The relative intensity of the observed excitation bands significantly changes as a function of the annealing temperature. Especially, the intensity ratio I_{HS}/I_{LS} between the $5d_1$HS and $5d_1$LS absorption bands increases as the annealing temperature decreases, being equal to 0.01, 0.28 and 1.76 for 1000, 900 and 400 °C, respectively. Partially, this effect could be related to mixing the 5d orbital with anion ligand orbitals that reduces the spin purity of the state. As a result, the oscillator strength of the spin forbidden transition relative to that of the spin allowed transition increases. This effect is known to significantly influence the I_{HS}/I_{LS} ratio. However, it must be emphasized that the interpretation of PLE results, especially the PLE intensities, is more complex than the interpretation of absorption results. In general, the PLE signal intensity, I_{PLE}, can be described as $I_{PLE} \sim P_{abs}P_{rel}P_{em}$ [16], where P_{abs},

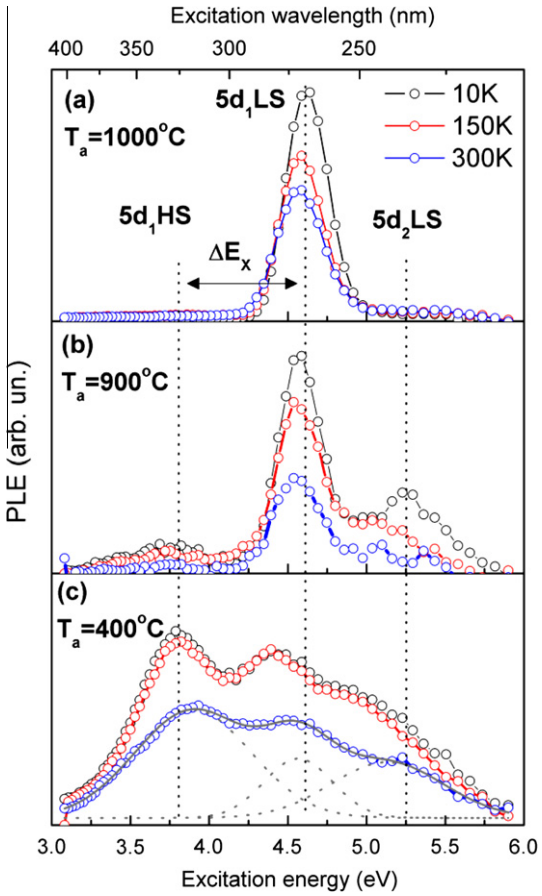

Fig. 2. Photoluminescence excitation measured as a function of temperature for samples annealed at (a) 1000, (b) 900 and (c) 400 °C. In the case of 400 °C sample, for 300 K, an exemplary fit with Gaussians is shown (also a slight offset from zero can be seen).

P_{rel}, P_{em} denote the probability of photon absorption, the probability of relaxation from a given excited state to the emitting state, and the probability of photon emission, respectively. It is evident that in order to observe the PLE signal, the system must reach the emitting state first. However, P_{rel} may differ for various excited states. In particular, P_{rel} may be different for $5d_1$HS and $5d_1$LS states, which could influence the I_{HS}/I_{LS} ratio. This is especially visible in the case of T_a = 400 °C sample, where the spin-forbidden transition band is stronger than the spin-allowed. We related this effect to the enhanced nonradiative recombination from the $5d_1$LS state which influences PLE bands intensities.

Moreover, Fig. 2 shows that for T_a = 400 °C the excitation bands are very broad and strongly overlap. On the other hand, when the annealing temperature increases, the excitation bands sharpen and become well resolved. For T_a = 1000 °C, the most intensive excitation occurs through spin-allowed $4f^8 \rightarrow 5d_14f^7$ transition ($5d_1$LS), whereas side-band intensities are reduced almost completely. This result shows that the phase transformation induced by the annealing significantly influences the excitation mechanism of Tb^{3+} ions.

It has been recently well established that the isotropic exchange interaction between the 5d electron spin state and the total spin of the electrons in the $4f^{n-1}$ core splits the energy of the first spin allowed and the first spin forbidden f–d transition about 1 eV [17]. The energy difference ΔE_x between spin allowed and spin forbidden Tb^{3+} states was studied theoretically for various crystals. In the case of $YAlO_3$, it was calculated [18] that if the Tb^{3+} ion occupies the Y^{3+} site, the ΔE_x value equals to 0.76 eV (6180 cm^{-1}). In the investigated case, the energy splitting between $5d_1$HS and $5d_1$LS states is 0.80 eV and 0.81 eV for samples annealed in 900 and 1000 °C, respectively (see Fig. 2). It should be noted here that these are the samples where $YAlO_3$ phase was detected by the X-ray diffraction technique. As it can be seen, the theoretical predictions agree quite well with our experimental results, suggesting that in the samples annealed at 900 and 1000 °C, Tb ions occupy Y site in the $YAlO_3$ crystal lattice. Furthermore, for the sample annealed at 400 °C, ΔE_x decreases to 0.62 eV. Since for T_a = 400 °C the xerogel is amorphous, the significant change of ΔE_x value indicates a change of the Tb^{3+} ion environment.

It is well known that with increasing temperature, the absorption lines of purely electronic transitions have much broader linewidth [19] than the one brought about by inhomogeneous broadening. The actual full-width at half maximum (FWHM) is broadened by the electron–phonon interaction. Therefore, the strength of the electron–lattice coupling can be examined by measuring the absorption spectra as a function of temperature. In the present study, we have used the excitation spectra, which are not exactly the same as the absorption spectra and therefore the obtained coupling parameters may be slightly overestimated. However, we have shown previously [20] that in the case of a strong electron–lattice interaction, the excitation data may be successfully used to estimate the electron–lattice coupling strength and to compare properties of samples deposited at various technological parameters.

In order to estimate the strength of the electron–lattice coupling, the main excitation bands were fitted with Gaussian line shape functions and the FWHM have been extracted from the fit as a function of temperature. In the case of T_a = 400 °C sample, beside Gaussian bands, also a slight offset was accounted for in order to improve the fit quality. This offset may be related to an additional excitation mechanism present in T_a = 400 °C sample, such as defects-originated energy transfer. However, in comparison with direct excitation through f–d transitions (Gaussian bands) this mechanism is negligible and therefore was excluded from further discussion for clarity reasons. Furthermore, only the $5d_1$LS band was chosen for further analysis since this is the strongest excitation band that remains visible for all the samples, allowing to perform a comparison of samples.

The extracted FWHM as a function of temperature are shown in Fig. 3, for structures annealed at 1000, 900 and 400 °C, respectively. It can be seen that the FWHM increases with temperature. In the next step, the obtained data were used to estimate the coupling of 5d electrons of the Tb^{3+} ions with the lattice vibrational modes. The estimations have been made according to the well-known Huang–Rhys model [21]. Assuming a Gaussian-like line shape of the absorption band, the thermal broadening of the absorption band FWHM follows the relation below:

$$\mathrm{FWHM}_{\mathrm{hom}}(T) = \hbar\omega_{\mathrm{eff}}\sqrt{8\ln 2S\coth\left(\frac{\hbar\omega_{\mathrm{eff}}}{2kT}\right)} \quad (1)$$

where S is a unitless measure describing the strength of the electron–lattice coupling known as the Huang–Rhys parameter and $\hbar\omega_{\mathrm{eff}}$ is the effective phonon energy. We used Eq. (1) to fit the experimental data obtained for crystalline samples (annealed at 1000 °C and 900 °C). Moreover, in a disordered material (i.e. amorphous), the absorption band can be additionally broadened due to the heterogeneity of Tb^{3+} ions environment. This leads to the so-called "inhomogeneous" broadening contribution, $\mathrm{FWHM}_{\mathrm{inh}}$, which is generally temperature-independent. In this situation, the measured FWHM should be modified [22]:

$$\mathrm{FWHM}^2(T) = \mathrm{FWHM}^2_{\mathrm{hom}}(T) + \mathrm{FWHM}^2_{\mathrm{inh}} \quad (2)$$

Since the structure of the sample annealed at 400 °C is entirely amorphous, the heterogeneity of Tb^{3+} binding sites is important, leading to additional broadening of the absorption band. Therefore,

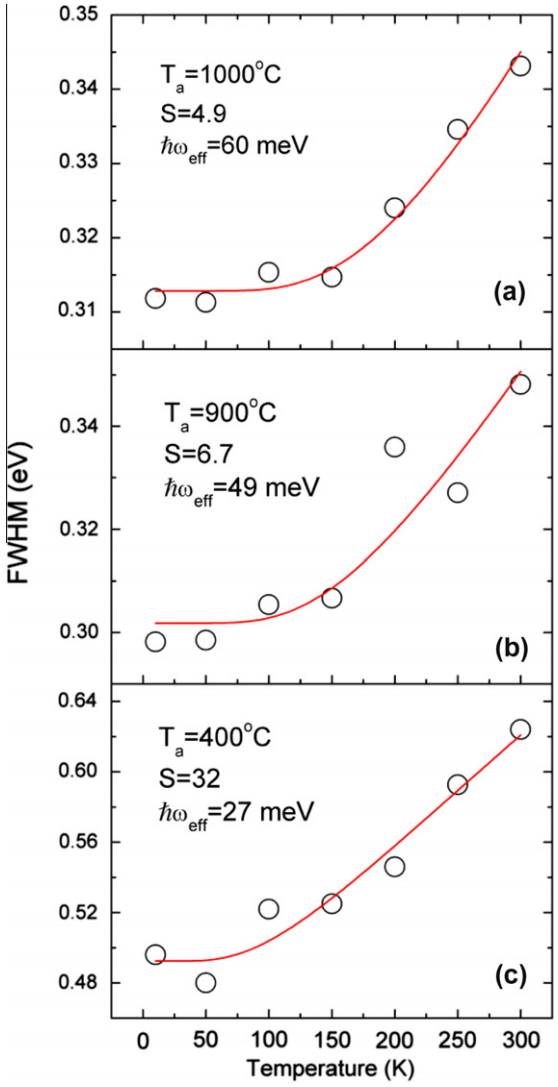

Fig. 3. FWHM of $5d_1$LS absorption band of Tb^{3+} ions calculated for samples annealed at (a) 1000, (b) 900 and (c) 400 °C. Fit to Huang–Rhys model has been also shown (solid line) together with the extracted parameters.

to fit the experimental data obtained for this sample, we used Eq. (2), including $FWHM_{inh}$ as a fit parameter. From the fit, we obtained $FWHM_{inh}$ = 300 meV. The large value of the inhomogeneous broadening is due to the amorphous structure of the 400 °C sample, where Tb^{3+} ions can exist in many different environments. It should also be mentioned that the experimental data obtained for 400 °C sample could be fitted with Eq. (1) instead of Eq. (2), resulting in a comparable S and a slightly higher $\hbar\omega_{eff}$ value. Nevertheless, we would like to emphasize that the model selection does not change the obtained tendencies and interpretation. We chose Eq. (2) to fit the 400 °C data, since this model accounts for the sample heterogeneity.

Fig. 3 shows the obtained results (solid lines) together with the extracted parameters. The S values of 4.9, 6.7 and 32 were obtained for samples annealed at 1000, 900 and 400 °C, respectively. It can be seen that Huang–Rhys parameter increases as the annealing temperature drops. This means that the strength of the electron–lattice coupling is changed after annealing. Moreover, the high value of the obtained Huang–Rhys parameters indicate a very strong electron–lattice coupling ($S > 1$). This is not surprising, since, in general, the $4f^n \leftrightarrow 4f^{n-1}5d$ transitions are characterized by a much stronger electron–lattice coupling than $4f^n \leftrightarrow 4f^n$ transitions. The typical Huang–Rhys factors for the f–d transitions range from 1.5 to 5, but some less typical values of the order of 22–32 have also been reported [23,24].

The effective phonon energies $\hbar\omega_{eff}$ obtained from the fit are 60 meV, 49 meV and 27 meV for samples annealed at 1000, 900 and 400 °C, respectively. It can be seen that the effective phonon energy decreases with the annealing temperature drop. Furthermore, in the configurational coordinate model, we may define the reorganization energy [25] E_R as $E_R = S\hbar\omega_{eff}$. This is the energy that must be dissipated for vibrational relaxation. Using the harmonic approximation, the reorganization energy is related to the effective force constant C_{eff} by the well known equation $E_R = (C_{eff}\cdot q^2)/2$, where q is the maximum displacement of the excited and ground state parabolas in the configurational coordinate diagram. We may therefore combine q and E_R in one equation:

$$q = \sqrt{\frac{2S\hbar\omega_{eff}}{C_{eff}}} \tag{3}$$

Since the reorganization energy increases when the annealing temperature drops (more energy needs to be dissipated), we may expect that the Tb^{3+} ion environment changes (C_{eff} or q changes with annealing temperature). This seems to be a sensible conclusion since the annealing changes the crystal phase of the matrix. One of the possible explanations of this effect is preferential creation of Tb_2O_3 phase in the case of the amorphous (400 °C) sample. This is plausible since the enthalpy of formation of Tb_2O_3 clusters is about $\Delta H = -1865$ kJ/mol [26], and therefore the process is strongly exothermic. On the other hand, in 900 and 1000 °C samples, $YAlO_3$ crystal phase is formed, resulting in the substitution of Tb into Y sites. In the case of Tb_2O_3 clusters, Tb ions are 6-fold coordinated with oxygen [27] while in the case of $YAlO_3$ the coordination is 12-fold [28]. This influences the Tb–O bond strength. In the case of Tb_2O_3, the Tb–O force constant C_{eff} is about 110 N/m [29], which yields q = 0.5 Å, according to Eq. (3) (400 °C sample). In the case of $YAlO_3$, assuming substitution of Y with Tb, the force constant C_{eff} is about 45 N/m [28], which yields q = 0.45 Å (1000 °C sample). Since the amplitude of atomic oscillations in a crystal is of the order of 0.1 Å (strongly depending on the crystal structure), the obtained values of q are consistent. Moreover, the above estimation shows that q may be comparable for 400 and 1000 °C samples, despite the fact that E_R differs significantly. This may be also a physical justification for the large S value obtained for 400 °C sample. Nevertheless, the above considerations should be treated rather cautiously due to the model simplicity.

It should also be pointed out that according to the model developed by Dorenbos [17], there is a correlation between the exchange splitting energy ΔE_x and the so-called spectroscopic polarizability α_{calc} of anion ligands. The polarizability α_{calc} is a measure of the amount of covalency between the 5d orbital and anion ligand orbitals. As shown by Dorenbos [17], the size of the exchange splitting ΔE_x decreases as the covalency between 5d orbital and ligand orbitals increases (polarizability α_{calc} increases). On the other hand, the increase in covalency can be considered as an increase of the spatial extension of the electronic wavefunctions of the metal ion and ligands [30] (the 5d electron is more delocalized over the ligands). This leads to a larger overlap between the ligand and the ion 5d orbitals. Simultaneously, the average distance between the electron and the Ln^{3+} nucleus increases because of the partial donation of the electronic density from the ligands. In this way, the electron–lattice coupling strength and, consequently, the Huang–Rhys parameter S increases [30] with increasing α_{calc} (ΔE_x decreases).

Fig. 4 shows normalized PL decay measured at λ_{EM} = 544 nm ($^5D_4 \rightarrow {}^7F_5$ transition) for 4.59 eV excitation ($5d_1$LS absorption

band) for samples annealed at 1000, 900 and 400 °C. In general, the obtained decay curves are non-single exponential, especially in the case of T_a = 400 °C sample. The non-exponential decays are characteristic for disorder materials [31] with complex interactions, where various effects influence the relaxation process (i.e. relaxation via defect states, presence of energy transfer interactions, various Tb^{3+} sites etc.). The very strongly non-exponential decay in the T_a = 400 °C sample indicates significant disorder and complexity, which is expected for an amorphous material. Nevertheless, for the purpose of sample comparison the average decay time was evaluated according to the following equation:

$$\langle \tau \rangle = \frac{\int I_{PL}(t) t dt}{\int I_{PL}(t) dt} \quad (4)$$

The values of 3841, 3409, and 1532 μs were obtained for samples annealed at 1000, 900 and 400 °C, respectively. The long decay times are characteristic for $^5D_4 \rightarrow {}^7F_5$ transition. Moreover, it was found that the average decay time rapidly drops when the annealing temperature decreases.

Table 1 summarizes parameters obtained for structures annealed at various temperatures. Moreover, we also showed spectroscopic polarizabilities of anion ligands, α_{calc}, calculated according to the linear relation shown by Dorenbos. We would like to emphasize that α_{calc} values should be considered only as an estimation, introduced in order to explain the observed tendencies.

Below we summarize the obtained experimental results and explain the observed effects:

1. It can be seen in Tab. 1 that when the annealing temperature drops, the electron–lattice coupling strength S increases and the exchange splitting energy ΔE_x decreases. This indicates that the amount of covalency between the 5d orbital and anion ligand orbitals (polarizability α_{calc}) significantly rises with T_a drop. We relate this effect to the change of the Tb^{3+} environment in YAP:Tb^{3+}/PAA xerogels annealed at different temperatures. Moreover, since the spectroscopic polarizability is related to cation electronegativity χ (or average electronegativity χ_{av} [32] for nonbinary compounds) as $\alpha_{calc} \sim 1/\chi^2$ [32], we expect that the Tb^{3+} electronegativity increases as a function of the annealing temperature. We relate this effect to the substitution of Tb ions into Y sites in $YAlO_3$ lattice in the case of T_a = 900 and 1000 °C samples. The Y site is 12-fold coordinated with oxygen atoms, which brings a quite high electronegativity (χ_{av} = 1.415 for $YAlO_3$ and χ_{av} = 1.355 for $TbAlO_3$). On the other hand, for T_a = 400 °C sample, the electron–phonon coupling S is very large, indicating a significant drop in the Tb^{3+} electronegativity. At the moment, the predominant chemical surrounding of Tb atoms in T_a = 400 °C sample remains unknown. However, the drop in electronegativity (rise of α_{calc}) suggests at least two possibilities: (a) a high coordination of Al around Tb atoms (this should decrease χ_{av} since Al is a less electronegative element than O) or (b) the creation of amorphous Tb_2O_3 complexes (with χ = 1.1). Noteworthy, as shown for glasses, where Tb_2O_3 complexes are often formed, the majority of Tb ions are coordinated to 6 oxygens [27]. This is a significant difference in comparison to 12-fold coordination with oxygens in $YAlO_3$ (assuming substitution of Y with Tb), which should result in an increased covalency. Indeed, it was shown that the degree of covalency of Tb–O bonds is higher in glasses when compared to other hosts [33]. This may explain the high electron–lattice coupling strength obtained for the amorphous (400 °C) sample.
2. The effective phonon energies obtained for samples annealed at 1000 and 900 °C correspond to the longitudinal (LO) or transverse (TO) phonon energies of the orthorhombic perovskite $YAlO_3$ [28,34] and therefore indicate coupling to the optical phonon branch. This is exactly what could be expected when the Tb ions substitute Y sites in $YAlO_3$ crystal. Contrary to this, the phonon energy obtained for T_a = 400 °C sample is smaller than typical LO/TO lattice phonon energy and the phonon energy is therefore attributed to a local vibrational mode. This result could also be expected, since the structure of T_a = 400 °C sample is entirely amorphous and the collective lattice vibrations are no longer present.
3. The observed increase of the electron–lattice coupling strength S indicates that the vibronic transition probability is higher for samples annealed at lower temperatures. This increases the nonradiative decay rate (multiphonon relaxation) and leads to a shorter mean PL lifetime. What is more, we can expect that the differential expansion of the 5d orbitals relative to the 4f orbitals could reduce the $< 4f|r|5d >$ dipole matrix element [35]. This effect and the simultaneous increase of the nonradiative decay rate explain the PL intensity drop observed for samples annealed at lower temperatures. It should also be emphasized that some defect-related nonradiative recombination is also possible in the case of T_a = 400 °C sample. We cannot exclude that, at least partially, such processes lead to a shorter PL lifetime. Another possibility is Tb clustering in the amorphous structure of T_a = 400 °C sample, leading to ion-ion interactions. The strongly non-exponential character of the decay curve measured for 400 °C sample suggests that the relaxation is indeed very complex, probably involving various relaxation channels. This remains an open question requiring further investigation.

Table 1
Parameters extracted from experimental data fitting. Values of ΔE_x, I_{HS}/I_{LS} and α_{calc} were calculated at T = 10 K.

T_a (°C)	S	$\hbar\omega_{eff}$ (meV)	$<\tau>$ (μs)	ΔE_x (eV)	I_{HS}/I_{LS}	α_{calc} (10^{-30} m^3)
1000	4.9	60	3841	0.81	0.01	2.38
900	6.7	49	3409	0.80	0.28	2.44
400	32.0	27	1532	0.62	1.76	3.46

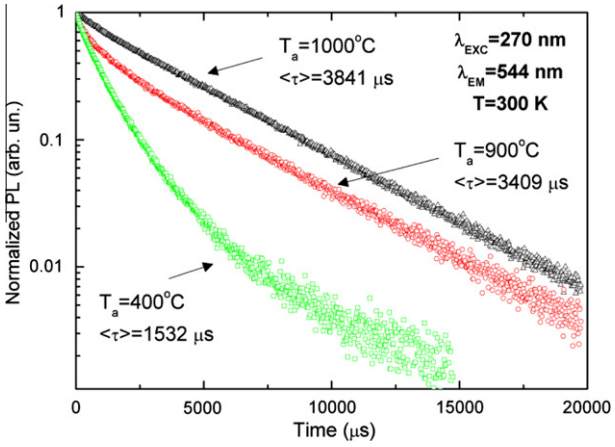

Fig. 4. Photoluminescence decay measured for $^5D_4$–$^7F_5$ transition. The excitation was through $5d_1$LS state.

4. Conclusions

To sum up, the Tb^{3+} doped YAP xerogels were deposited on porous anodic alumina substrates and annealed at various temperatures (400, 900 and 1000 °C). An intense green emission was observed for all the samples with the strongest emission band centered at 544 nm ($^5D_4 \rightarrow {}^7F_5$ transition). The strongest emission

intensity was obtained for the sample annealed at 1000 °C. It was found that the dominant excitation band is through spin allowed $4f^8 \rightarrow 5d_14f^7$ transition. Moreover, it was shown that the transition is strongly coupled to lattice vibrational modes. The electron–lattice coupling strength was found to increase with the annealing temperature drop. This effect was ascribed to changes of the amount of covalency between the 5d orbital and anion ligand orbitals due to the change of the Tb^{3+} environment. The electron–lattice coupling was also found to affect the relaxation kinetics, leading to a shorter mean PL lifetime.

Acknowledgments

In Poland, this study was financed by the National Science Center as a research project NN507321240.

References

[1] N.V. Gaponenko, Synthetic Metals 124 (2001) 125.
[2] W. Chen, J.-S. Wu, X.-H. Xia, ACS Nano 2 (2008) 959.
[3] X. Fu, B. Zhang, X. Kang, J. Deng, C. Xiong, T. Dai, X. Jiang, T. Yu, Z. Chen, G.Y. Zhang, Optics Express 19 (2011) A1104.
[4] Y. Su, G.T. Fei, Y. Zhang, P. Yan, H. Li, G.L. Shang, L.D. Zhang, Materials Letters 65 (2011) 2693.
[5] A.A. Lutich, S.V. Gaponenko, N.V. Gaponenko, I.S. Molchan, V.A. Sokol, V. Parkhutik, Nano Letters 4 (2004) 1755.
[6] N.V. Gaponenko, I.S. Molchan, G.E. Thompson, V. Lambertini, P. Repetto, Journal of the Society for Information Display 11 (2003) 27.
[7] C. Hong, T.-T. Tang, C.-Y. Hung, R.-P. Pan, W. Fang, Nanotechnology 21 (2010) 285201.
[8] P. Nachimuthu, R. Jagannathan, Journal of the American Ceramic Society 82 (1999) 387.
[9] A.F. Campos, A. Meijerink, C.d.M. Donegá, O.L. Malta, Journal of Physics and Chemistry of Solids 61 (2000) 1489.
[10] M.D. Marcantonatos, Journal of the Chemical Society, Faraday Transactions 82 (2) (1986) 381.
[11] N.V. Gaponenko, V.S. Kortov, N.P. Smirnova, T.I. Orekhovskaya, I.A. Nikolaenko, V.A. Pustovarov, S.V. Zvonarev, A.I. Slesarev, O.P. Linnik, M.A. Zhukovskii, V.E. Borisenko, Microelectronic Engineering 90 (2012) 131–137.
[12] A. Podhorodecki, M. Banski, J. Misiewicz, J. Serafinczuk, N.V. Gaponenko, Journal of the Electrochemical Society 157 (2010) H628.
[13] A. Podhorodecki, M. Nyk, J. Misiewicz, W. Strek, Journal of Luminescence 126 (2007) 219.
[14] P. Dorenbos, Journal of Luminescence 91 (2000) 91.
[15] R. Turos-Matysiak, W. Gryk, M. Grinberg, Y.S. Lin, R.S. Liu, Journal of Physics: Condensed Matter 18 (2006) 10531.
[16] A. Podhorodecki, M. Nyk, J. Misiewicz, W. Strek, Proceedings of SPIE, San Diego, CA, USA, 2006, 63210O–63210O–7.
[17] P. Dorenbos, Journal of Physics: Condensed Matter 15 (2003) 6249.
[18] J. Shi, S. Zhang, Journal of Physics: Condensed Matter 15 (2003) 4101.
[19] A. Ellens, H. Andres, M.L.H. ter Heerdt, R.T. Wegh, A. Meijerink, G. Blasse, Physical Review B 55 (1997) 180.
[20] A. Podhorodecki, P. Gluchowski, G. Zatryb, M. Syperek, J. Misiewicz, W. Lojkowski, W. Strek, Journal of the American Ceramic Society 94 (2011) 2135.
[21] K. Huang, A. Rhys, Proceedings of the Royal Society of London. Series A, Mathematical and Physical Sciences 204 (1950) 406.
[22] G. Zucchelli, F.M. Garlaschi, R.C. Jennings, Biochemistry 35 (1996) 16247.
[23] D.W. Cooke, B.L. Bennett, K.J. McClellan, J.M. Roper, M.T. Whittaker, Journal of Applied Physics 87 (2000) 7793.
[24] L.C. Nehru, K. Marimuthu, M. Jayachandran, C.-H. Lu, R. Jagannathan, Journal of Physics. D. Applied Physics 34 (2001) 2599.
[25] Z. Pan, J.P. Wicksted, H. Liu, Physical Review B 48 (1993) 844.
[26] E.H.P. Cordfunke, R.J.M. Konings, Thermochimica Acta 375 (2001) 65.
[27] E.B. Clark, R.N. Mead, G. Mountjoy, Journal of Physics Condensed Matter 18 (2006) 6815.
[28] H.C. Gupta, P. Ashdhir, Journal of Solid State Chemistry 146 (1999) 287.
[29] A. Ubaldini, M.M. Carnasciali, Journal of Alloys and Compounds 454 (2008) 374.
[30] C. de M. Donega, A. Meijerink, G. Blasse, Journal of Physics: Condensed Matter 4 (1992) 8889.
[31] G. Zatryb, A. Podhorodecki, X.J. Hao, J. Misiewicz, Y.S. Shen, M.A. Green, Optics Express 18 (2010) 22004.
[32] P. Dorenbos, Physical Review B 65 (2002) 235110.
[33] B.C. Jamalaiah, M.V. Vijaya Kumar, K. Rama Gopal, Physica B: Condensed Matter 406 (2011) 2871.
[34] R. Vali, Journal of Luminescence 127 (2007) 727.
[35] G.M. Williams, N. Edelstein, L.A. Boatner, M.M. Abraham, Physical Review B 40 (1989) 4143.